MDPI

Removal of Reactive Black 5 Azo Dye from Aqueous Solutions by a Combination of Reduction and Natural Adsorbents Processes

Wael Ben Mbarek [1], Jason Daza [1], Lluisa Escoda [1], Núria Fiol [2], Eloi Pineda [3], Mohamed Khitouni [4] and Joan-Josep Suñol [1,*]

1   Department of Physics, Campus Montilivi s/n, University of Girona, 17003 Girona, Spain
2   Department of Chemical Engineering, Campus Montilivi s/n, University of Girona, 17003 Girona, Spain
3   Department of Physics, Institute of Energy Technologies, Universitat Politècnica de Catalunya, 08019 Barcelona, Spain
4   Department of Chemistry, College of Science, Qassim University, Buraidah 51452, Saudi Arabia
*   Correspondence: joanjosep.sunyol@udg.edu

Abstract: In this study, a combined process of reduction and adsorption for the degradation of azo dye with nanocrystalline $Fe_{80}Si_{10}B_{10}$ powder as a reducing agent is analyzed. A mechanical alloying technique produced the powdered alloys needed for the redox process. The synthesized nanocrystalline structure favors the efficiency of the reduction step of Reactive Black 5 (RB5) azo dye. According to the UV-Vis analysis, the reductive process alone allowed for nearly complete color removal after 3 min of reaction. In this regard, the nanocrystallized FeSiB powder has excellent application potential in the first step of the reduction processes for degrading azo dye solutions. Indeed, the nanocrystalline FeSiB powder outperforms commercial Fe powders in terms of degradation efficiency because of the formation of multiple micro-batteries between the α-Fe solid solution and the Fe_3Si nanocrystalline phases, favoring the loss of electrons from iron and exhibiting different corrosion resistance. In the second step, the adsorption process, the efficient removal of intermediate undesired compounds from the reduction processes, principally aromatic amines, is analyzed. Different adsorbents, including wood, graphene oxide, activated carbon, and pine particles, were used. The results suggest that graphene oxide and activate carbon performed the best for secondary product adsorption following RB5 degradation. The current study could serve as a guide for environmental applications, such as industrial wastewater treatment, using metallic powders produced by high-energy mechanical alloying.

Keywords: nanocrystalline; mechanical alloying; degradation; adsorption

1. Introduction

Industrial dyes, as well as their by-products, are the main polluters of the waters that are discharged into the fluvial systems. Both are considered potentially toxic and carcinogenic and [1], consequently, they lead to harmful effects on the ecosystem [2]. Various reports are available which show the harmful effects of azo dyes on plants (plant growth and germination) [3]. At present, there are physical–chemical and biological methods to degrade dye wastewater, such as adsorption [4–6], ozonation [7,8], Fenton's reagent treatment [8], photocatalysis [9], reductive degradation [10–12], and microbial processes [13]. Adsorption, flocculation, electro-coagulation, precipitation, ozonation, and irradiation are examples of physical and chemical treatments. However, these processes may not be sufficient to remove dyes from effluent. The biological approach, for example, is inappropriate for removing color from dyes, since most of them are inorganic and harmful to the microorganisms utilized in the process. Physical approaches, including membrane filtering, ion exchange, and adsorption, have significant limitations: they operate best when

the volume of wastewater is small and can be further broken down into a few microscopic components that are difficult to digest [1], whereas the combination of some of these methods have been successfully applied to the treatment of various dyes [14]. Among these methods, a chemical reduction process is fast and easy to implement for industrial level dye removal. Currently, several reducing agents (with different microstructures) have been used for azo dye removal, including zero-valent iron (Fe^0) [15] and iron-based nanoparticles [16]. In this research, we report a very fast reductive degradation method for Reactive Black 5 dye based on Fe rich Fe-Si-B crystallized powder particles which were synthesized by mechanical alloying. Based on the reduction process, micro-batteries are created between the α-Fe phase and the Fe3Si phase, making it easier to donate electrons to the N=N bond and decolorizing the azo dye solution faster. On the other hand, the possibility of an Fe-based amorphous alloy with the nominal composition $Fe_{78}Si_9B_{13}$ as a catalyst for activating persulfate to create sulfate radicals (SO_4^-) is being investigated [17]. The redox stage is followed by an adsorption process using natural adsorbent agents.

The mechanical alloying technique (MA) has been shown to be capable of producing a variety of metastable phases, including amorphous and nanocrystalline materials. The MA process involves the repeated cold welding, fracturing, and rewilding of particles in a high-energy ball mill. In this work, the nanocrystalline metal powder from MA is used in the azo dye reduction process, and the chemical products derived from the reaction are then adsorbed using different natural adsorbents in order to observe their efficiency. The reduction of the azo group and the corresponding loss of color is analyzed using the ultraviolet-visible spectrophotometry (UV-Vis) technique. The qualitative chemical analysis of non-adsorbed chemical products is carried out using the liquid chromatography–mass spectrometry (LC–MS) technique. Therefore, the adsorption ability of the secondary products using different supports, such as graphene oxide, pine cone, wood, activated carbon, and cotton, are investigated. In addition, the kinetic study of dye degradation with Fe-Si-B nanoparticles is performed.

2. Materials and Methods

2.1. Materials

Fe (99.97% purity, mean particle size <10 μm), Si (99.9% purity, mean particle size <2–5 μm), and B (99.7% purity, mean particle size <10 μm) were supplied by China New Metal Materials Technology Company (Dongguan, China). Anionic dye RB5 ($C_{26}H_{21}N_5Na_4O_{19}S_6$) (purity of 95%, Color Index 20,505; CAS number 17095-24-8) was supplied by Sigma-Aldrich (St. Louis, MO, USA). The adsorbents were selected to be eco-friendly and were applied without pre-treatment, including natural sub-products such as wood flakes, pine powder, and cotton, as well as powdered activated carbon (Alpha Aesar (Haverhill, MA, USA), Ash 4% max, ref.:74440-44-10), and graphene oxide (Aldrich, ref.:796034-1G).

2.2. Production of Fe Based Alloy

The mixtures of $Fe_{80}Si_{10}B_{10}$ (at.%) powders are prepared in proportions corresponding to the nominal composition from the elemental powders by using a planetary ball mill (Type P7) under Ar atmosphere over 50 h. Ball milling experiments are carried out in a hardened steel container. The ball-to-powder weight ratio (Q) is 2:1, and the milling speed (ω) is adjusted to 600 rpm. The milling sequence is selected to be 10 min of milling followed by a 5 min idle period, to prevent both sticking of the powder to the container walls and the balls, as well as powder agglomeration during milling.

2.3. Preparation of Reactive Black 5 Solution

Reactive Black 5 was used in this study as the model of azo textile dye, without any further purification process. Its structure is given in Figure 1, with a molecular weight of 991.82 g mol^{-1}. It has a maximum absorbance wavelength of 597 nm. To assess the colorant degradation process, a solution of RB5 was prepared by using 200 mg of commercial RB5

powder in 1 L of distilled water. In each experiment, 0.04 g of adsorbent was weighted and added to 20 mL of dye solution.
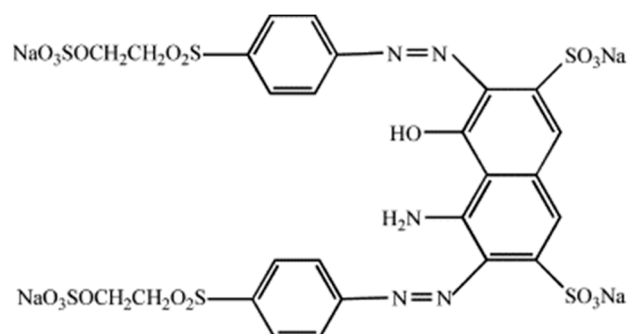
Figure 1. Chemical structure of the diazo dye Reactive Black 5.

2.4. Experimental Analysis Methods

　　The structure of the FeSiB powders was characterized by X-ray diffraction measurements using Siemens D-500 equipment with Cu-Kα radiation. The size of the crystallites, the lattice strains, and the lattice parameter are calculated based on the Rietveld method using the MAUD program [18]. The morphology and the chemical composition of the mechanically alloyed powder, before and after the reduction process, are examined by scanning electron microscopy (SEM) in a DSM960A ZEISS microscope in secondary electron mode, operating at a voltage of 15 kV. The SEM is equipped with a Vega Tescan energy dispersive X-ray spectrometry (EDS) analyzer. The reduction experiments are conducted in a 20 mL RB5 aqueous solution with an initial concentration of 200 mg/L by using 0.1 g of reactant and continuous agitation. Samples are removed and filtered at regular time intervals, and the absorbance between 200 and 800 nm is measured by spectrophotometry (Shimadzu 2600 UV-visible) with the aim of evaluating the efficiency of the process as a function of time. The powder collected after the reduction stage is analyzed using the Fourier transform infrared spectroscopy (FTIR) spectrum to determine the presence of functional groups in the extract.

　　To study the adsorption ability of the reaction products resulting from the reduction, the experiments are designed using natural adsorbents and comparing their efficiency with chemical adsorbents such as graphene oxide and activated carbon. Natural adsorbents, such as pine cone, wood, and cotton, were used. The adsorption experiments were conducted using 0.04 g of adsorbent into 20 mL of the supernatant solution after the reduction reaction and continuously agitated for 1 h. Samples were removed and filtered, and the absorbance between 200 and 800 nm was measured by spectrophotometry. The main focus is the 200 to 400 nm region in order to analyze the adsorption efficiency of the aromatic derivatives. In order to carry out a qualitative study of residual chemical products, the organic compounds from the RB5 degradation, reduction and adsorption, are analyzed by high-performance liquid chromatography (HPLC) (Agilent, Santa Clara, CA, USA) coupled with tandem mass spectrometry (LC-MS/MS Bruker, Billerica, MA, USA) in a Beckman Gold chromatograph fitted with a Proshell 120 Pheny Hexyl column at room temperature.

3. Results and Discussion

3.1. Characterization of Nanocrystalline FeSiB Powders

　　The XRD diffraction pattern of FeSiB powders before the reduction process is shown in Figure 2. One can observe that after 50 h of milling, two crystalline phases with different percentage are present. The first most relevant crystalline phase can be indexed as a solid solution of α-Fe (space group Im-3m), and the second phase is Fe_3Si (space group Fm-3m). The crystallographic parameters (lattice parameter, a, crystalline size, L, and micro strain, ε) have been calculated by Rietveld refinement (applying MAUD software, version 2.8) and are presented in Table 1. As can be seen in the table, both phases are nano-crystalline, with

an 88.8% of α-Fe solid solution and a calculation deviation given by the GoF of 1.315. The calculated values of crystallite sizes were 10.2 and 13.3 for the solid solution and Fe_3Si, respectively. The corresponding lattice micro-strains are around 0.5 and 0.6% for the α-Fe solid solution and the Fe_3Si phase, respectively. This nanocrystalline structure can be characterized by a high grain boundary volume fraction, which subsequently promotes an improving effect on the reactivity of the FeSiB powders in the solid state.
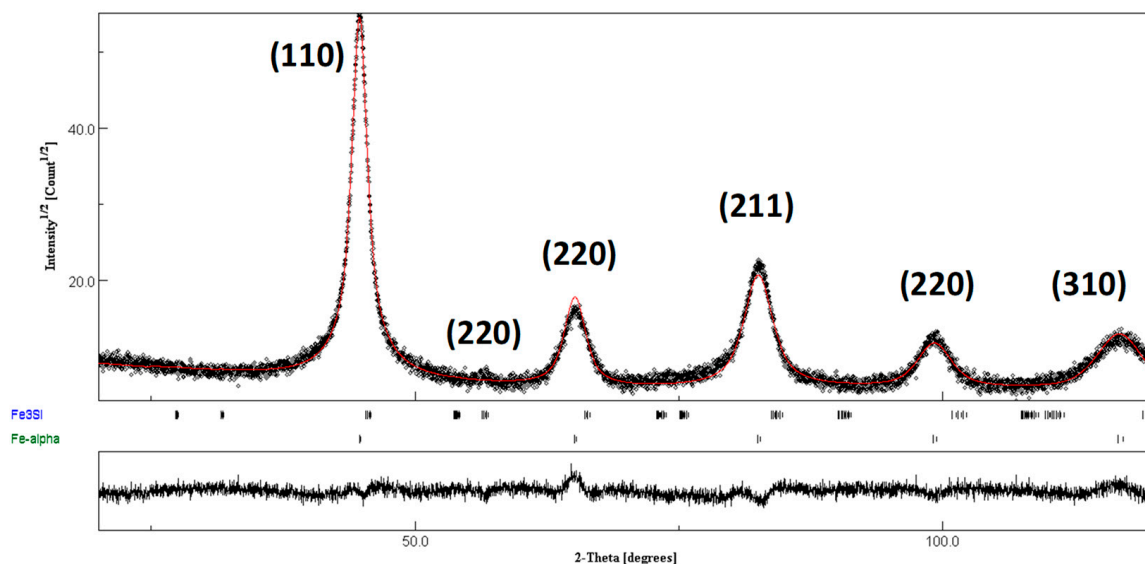
Figure 2. XRD diffraction pattern of the ball-milled $Fe_{80}Si_{10}B_{10}$ powder before the degradation of Reactive Black 5.

Table 1. Crystallographic parameters (lattice parameter, a, crystalline size, L, and micro strain, ε, calculated by Rietveld refinement of the $Fe_{80}Si_{10}B_{10}$ powder before the reduction process.

| Sample	Phase	%	a (Å)	Crystalline Size (nm)	Microstrain %	R_{wp}	R_{exp}	GoF
$Fe_{80}Si_{10}B_{10}$	α-Fe	88.8	2.862 (3)	10.2 (1)	0.52 (2)	11.481	8.730	1.315
	Fe_3Si	11.2	3.986 (4)	13.3 (11)	0.60 (1)			

Figure 3a,b illustrates the surface morphology of the ball-milled $Fe_{70}Si_{10}B_{10}$ powder before reduction. It is clear that the particle sizes show a relatively uniform distribution, and some aggregation can also be observed. As seen in the figure, their surfaces show many corrugations. The EDX analysis result shown in Figure 3c reveals that the as-produced ball-milled particles are composed of Fe and Si elements, while boron is not detected (due to technique limitations), with no significant traces of other elements. The ratio of Fe to Si is approximately equal to 80:10, which is in good agreement with the nominal composition of the alloy powder. Figure 3d displays the wide size distribution of the particles of the alloy, with an average diameter of 4.87 μm.

3.2. Decolorization of RB5 Aqueous Solution by Using Nanocrystalline FeSiB Powders

Figure 4a shows the UV absorption spectra for the RB5 solution, before and after the reduction process. The inset shows the appearance of the RB5 solution. The characteristic absorption peak at 597 nm corresponds to the "–N=N–" azo bonding. The typical wavelength of naphthalene and condensed ring aromatics above 300 nm can be also observed in the spectrum of the RB5 dye. The decline in the absorbance at 597 nm is attributed to the decolorization of RB5; however, a fracturing of all the molecules of the dye at the initial times is not observed, as is shown in the figure. Nonetheless, after 3 min of contact with the FeSiB alloy, the cleavage of the naphthalene, but not of benzene rings, is observed after

complete dye reduction. Gnanamoorthy et al. [19] reported that the decolorization of azo dyes by Fe3O4/rGO/ZnSnO3 nanocomposite using the halogen light irradiation technique is significantly less efficient and slower. The concentration of 10 mg of catalyst in the presence of aqueous methylene blue dye was reduced at 60 min, with a final decolorization of 60%. Moreover, in another recent work, Gnanamoorthy et al. [20] observed a 20 min degradation time with a 75% degradation percentage when 25 mg of amine-functionalized Bi2Sn2O7/rGO was added to a 1×10^{-3} M solution of methylene blue dye. When the initial dye concentration and the amount of powder per volume are considered, the decolorization process found for FeSiB is more efficient and faster than any other documented in the cited publications.
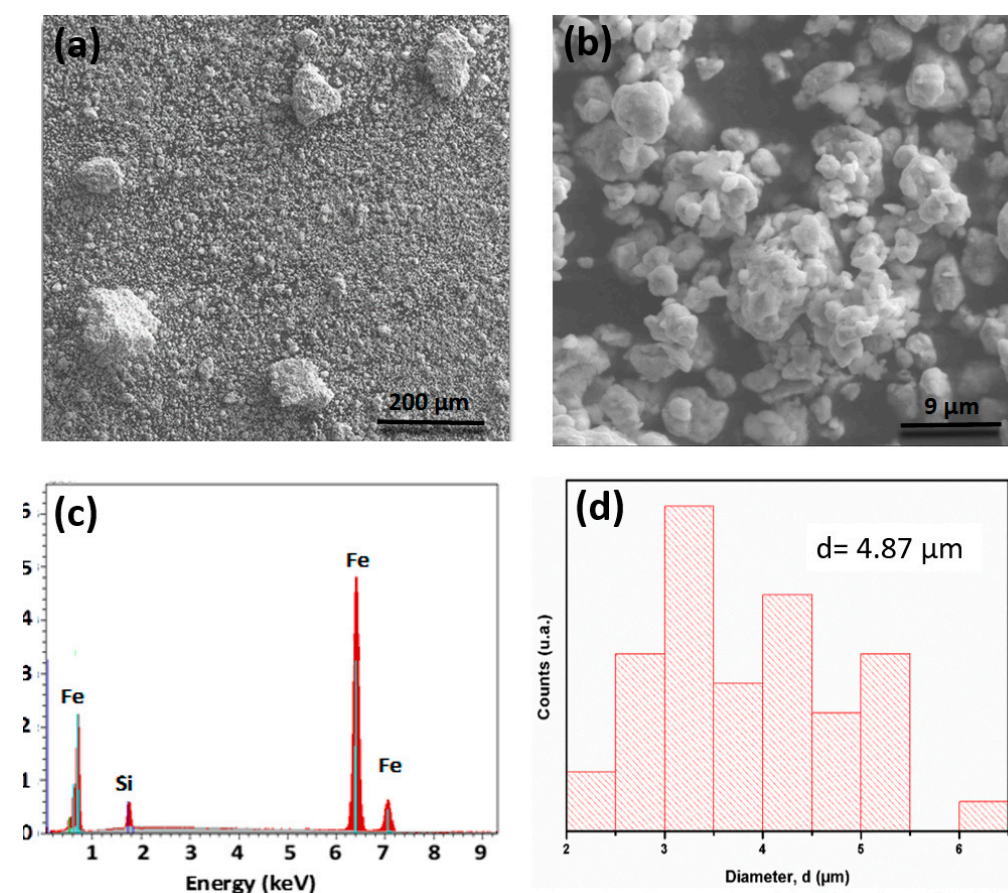
Figure 3. Particle morphologies (**a**,**b**) of the ball-milled $Fe_{80}Si_{10}B_{10}$ powder before the reduction process. (**c**) The nominal compositions as examined by EDX. (**d**) Distribution of particle sizes of the ball-milled powders.

The absorption band of benzene drifts towards lower wavelengths as a consequence of the fracture of naphthalene and the corresponding loss of the interaction between the two absorption signals. An increase in the intensity near 250 nm is evidence of the fracture of the double bond of the azo group and the formation of aromatic derivatives as new reaction products. The same results have been reported by Ben Mbarek et al. [11,21] in the case of the reductive degradation of Reactive Black 5 dye solution by Mn-Al and Ca-Al. The intensity of the characteristic absorption peak at 597 nm eventually decreased as the degradation proceeded, and the peak finally disappeared, indicating a complete decomposition of the RB5 molecule. The cleavage of the naphthalene and benzene rings in the experimental conditions is not studied in this work.
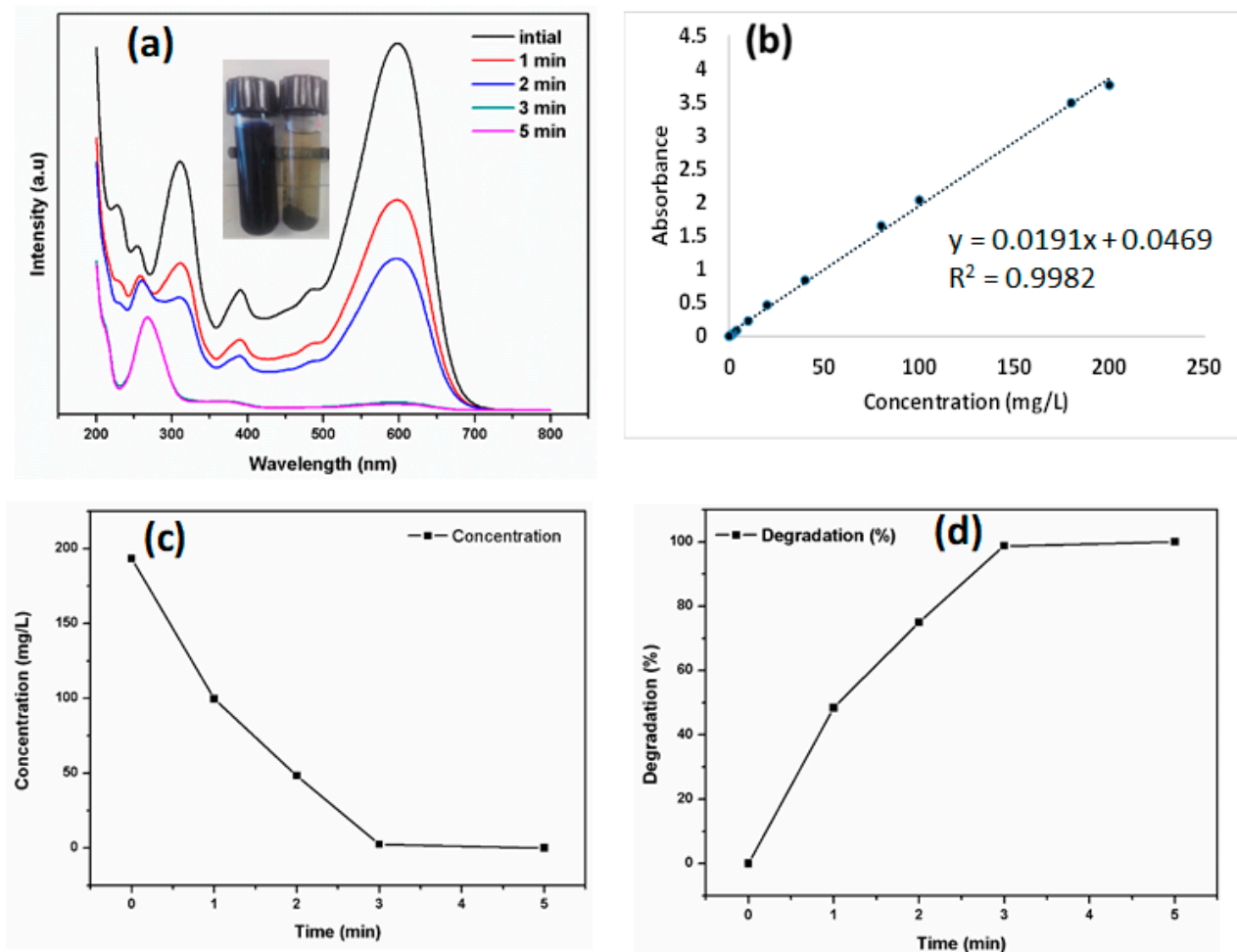
Figure 4. (**a**) UV absorption spectra for $Fe_{80}Si_{10}B_{10}$ alloy calibration curve of Reactive Black 5 at different times; (**b**) calibration curve of Reactive Black 5; (**c**) evolution of RB5 dye concentration after application of 0.1 g/20 mL of $Fe_{80}Si_{10}B_{10}$ powder; (**d**) dependence of the decolorization percentage on the reduction process induced by$Fe_{80}Si_{10}B_{10}$ powder.

It is known that the absorption intensity at 597 nm is linearly related to the RB5 concentration of solutions. To evaluate the dye reduction rate, calibration curves [22,23], with absorbance as a function of the concentration of dye patterns, were previously prepared (Figure 4b). The linear relationships between 1 to 200 mg·L^{-1} with good value of determination coefficient (R^2 = 0.9982), were observed. However, McBride et al. [24] discussed the errors inherent in all Beer's law plots and its limits of quantification and detection at high values of concentration. Indeed, the shifting slope of the line indicates that the resulting concentration error, C, would be modest at low concentrations and significant at high concentrations. By applying the following mathematical relationships [25], the value of the detection limit (LOD) and the value of the quantitative estimate limit (LOQ) are calculated as follows:

$$LOD = \frac{3\sigma}{S} \qquad (1)$$

$$LOQ = \frac{10\sigma}{S} \qquad (2)$$

where S = the slope for the standard curve, and σ = the standard deviation of 10 blank solutions. The results obtained for the values of LOD and LOQ are equal to 0.131308 mg·L^{-1} and 0.437694 mg·L^{-1}, respectively.

The decolorization ratio, D, is calculated using the following equation [26]:

$$D = \frac{C_0 - C_t}{C_0} \cdot 100\% \tag{3}$$

where C_0 is the initial concentration, and C_t is the concentration of RB5 at reaction time t. The representation of the residual concentration C_t as a function of time is shown in Figure 4c. The dependence of the decolorization ratio calculated from Equation (1) on time for the Fe$_{80}$Si$_{10}$B$_{10}$ powder is plotted in Figure 4d. Clearly, the Fe$_{80}$Si$_{10}$B$_{10}$ powder showed high efficiency, and it degraded 99% of the RB5 in 3–5 min.

The evaluation of the reaction efficiency at different temperatures, ranging from 25 to 50 °C, are shown in Figure 5. Thus, a very high at 50 °C was maintained by the degradation reaction (Figure 5a). The decay behavior is fitted by an exponential function, $I = I_0 + I_1 e^{-t/t_0}$ [27], where I is the normalized intensity of the absorption peak, I_0 and I_1 are the fitting constants, t is the degradation time, and t_0 is the time at which the intensity is diminished to e^{-1} of the initial state; it is derived by fitting the data points. Considering a thermally activated process for the reaction, we can evaluate the thermal activation energy barrier E_a with the Arrhenius-type equation, $t_0 = \tau_0 \times \exp{(E_a/RT)}$, where t_0 is a time pre-factor, and R is the gas constant. Figure 5b presents the Arrhenius plots of ln(t_0) as a function of 1/T for the degradation process of azo dye by using BM powder in the temperature range of 25–50 °C. The estimated ΔE value is 43.06 kJ mol^{-1}. Considering the fact that the activation energies for ordinary thermal reactions are usually between 60 and 250 kJ mol^{-1} [28], this result implies that the degradation of RB5 by the BM FeSiB required relatively low energy. The low activation energy, combined with the rapid decolorization, makes this material one of the most efficient for decolorization at ambient temperatures. The crystalline FeSiB powder, with favorable structures, shows degradation efficiencies comparable to or higher than those of the amorphous ZVI powders [29].
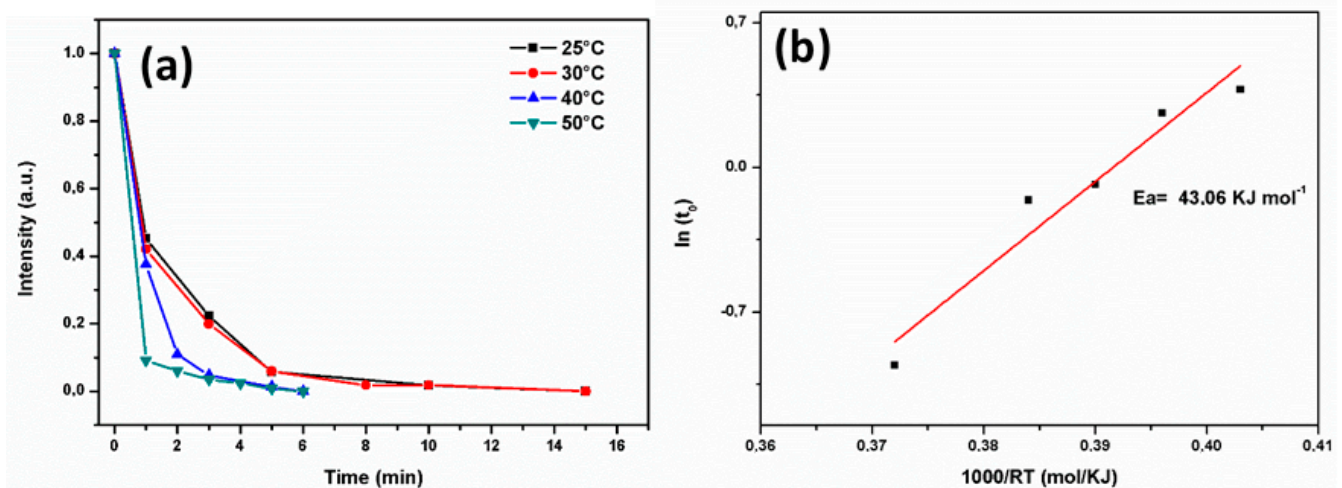
Figure 5. (**a**) The normalized UV absorption intensity at 597 nm versus the reaction time at different temperatures for the BM FeSiB powder. (**b**) Plot of the decay time (t_0) versus temperature. The solid lines are the fitting by Arrhenius-type equation to yield the activation energy.
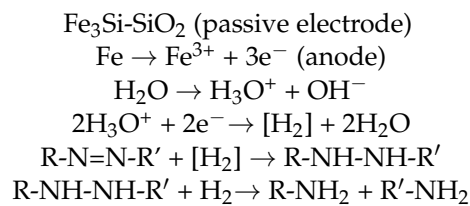
The status of FeSiB is monitored and the sediment phase compositions are identified. As is shown in Figure 6, the XRD spectrum of the FeSiB shows the appearance of new small peaks after the degradation reaction. These are identified as the γ-FeOOH phase, with sediments formed from the oxide exfoliation of the FeSiB powder surface. The existence of FeOOH indicates that Fe^0 is the reductive agent. During the process of reduction, micro batteries are generated between the α-Fe phase and the Fe$_3$Si phase. Thus, due to the micro-battery effect, the zero-valent iron Fe^0 in the α-Fe(Si,B) solid solution more easily donates its electrons to the N=N bond, and the azo dye solution is decolorized faster. Wang

et al. found that the numerous micro-batteries formed between the α-Fe (Si) and Fe_2B nano-crystalline phases in $Fe_{82.65}Si_4B_{12}Cu_{1.35}$ nano-crystalline alloy improved its efficiency in decolorizing the azo dye solution by about 20% (compared with the amorphous alloy or single nano-crystalline alloy) [30]. Zero valent iron (ZVI) is significantly less efficient that FeSiB; thus, the redox process is slower [31], even if the reduction is aided by elevated pH, an increase in temperature, or other additional parameters [32].
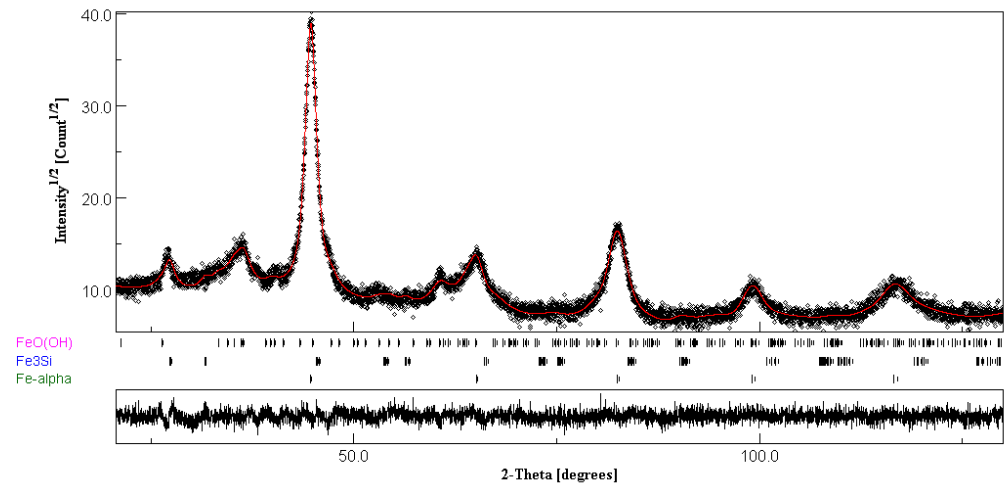
Figure 6. XRD diffraction pattern of the ball-milled $Fe_{80}Si_{10}B_{10}$ powder after the degradation of Reactive Black 5.

The Fe_3Si phase has a tendency to become passivated, with a corrosion potential of $E_{corr} = -0.37$ V in non-standard conditions [33], thus avoiding its subsequent oxidation. The passivation of the intermetallic phase would facilitate the oxidation of the α-Fe solid solution phase. The formation of the oxide-hydroxide FeOOH detected in the diffraction pattern suggests that Fe is oxidized to Fe^{3+} ($E^0_{Fe^{3+}/Fe} = 0.04$ V). The characteristic peak of SiO_2 ($2\theta = 21°$) from the Fe_3Si phase is not detected because its concentration is below the detection level of the X-ray diffraction equipment. At the initial pH conditions at which the reduction experiments are carried out (between 5 and 6), the H_3O^+ ions from the hydrolysis of water act as intermediaries for the reduction of the azo group. The activated hydrogen is retained on the metal surface, attacking the molecules of the azo dye that has previously been adsorbed by the metal powder. The proposed mechanism would be:

$$Fe_3Si\text{-}SiO_2 \text{ (passive electrode)}$$
$$Fe \rightarrow Fe^{3+} + 3e^- \text{ (anode)}$$
$$H_2O \rightarrow H_3O^+ + OH^-$$
$$2H_3O^+ + 2e^- \rightarrow [H_2] + 2H_2O$$
$$R\text{-}N\text{=}N\text{-}R' + [H_2] \rightarrow R\text{-}NH\text{-}NH\text{-}R'$$
$$R\text{-}NH\text{-}NH\text{-}R' + H_2 \rightarrow R\text{-}NH_2 + R'\text{-}NH_2$$

A schema of the micro batteries formed is given in Figure 7.

This mechanism is in agreement with the decrease in the percentage of the pre-existing phases detected by XRD (as shown in Table 2). The Fe_3Si phase experiences a slight decrease due to its passivation, while the phase that decreases the most is the solid solution α-Fe (Si,B) (from 88.8% to 77.7%). These results would justify the proposed mechanism, if compared with the results presented in Table 1.
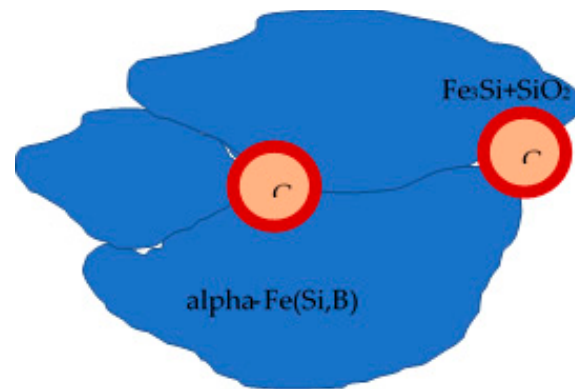
Figure 7. Scheme of the micro-batteries formed.

Table 2. Crystallography parameters (lattice parameter, a, crystalline size, L, and micro strain, ε) calculated by Rietveld refinement of $Fe_{80}Si_{10}B_{10}$ powder after the reduction process.

| Sample	Phase	%	a (Å)	Crystalline Size (Å)	Microstrain %	R_{wp}	R_{exp}	GoF
	α-Fe	77.7	2.864 (2)	106 (1)	0.053 (2)			
	Fe_3Si	9.9	3.987 (3)	76 (6)	0.058 (4)	11.783	9.897	1.191
$Fe_{80}Si_{10}B_{10}$			3.055 (7)					
	FeO (OH)	12.4	4.601 (2)	179 (1)	0.032 (3)			
			9.927 (3)					

The surface morphology for the Fe-Si-B powder after reaction with RB5 solutions is observed, as shown in Figure 8a. The morphological analysis also confirms the viability of the hypothesis for the formation of micro- or nanobatteries. The number of corrosion pits is much larger, and they are distributed all along the sample.
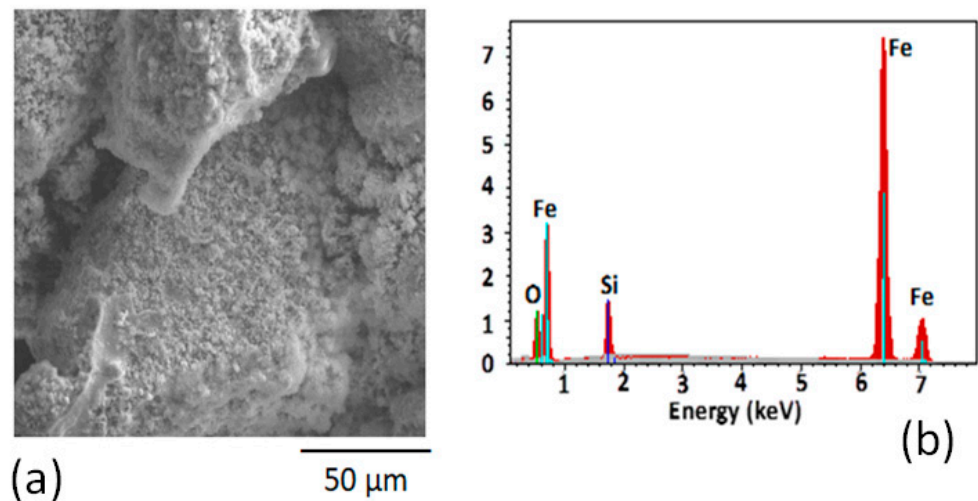
Figure 8. Particle morphology of (**a**) the ball-milled $Fe_{80}Si_{10}B_{10}$ powder after the reduction process; (**b**) the EDX microanalysis.

Regarding microanalysis, the EDX spectrum after the decoloring reaction is shown in Figure 8b.

Figure 9a,b show the typical FT-IR spectrum of the RB5 dye powder and the Fe-Si-B powder after the reduction process.
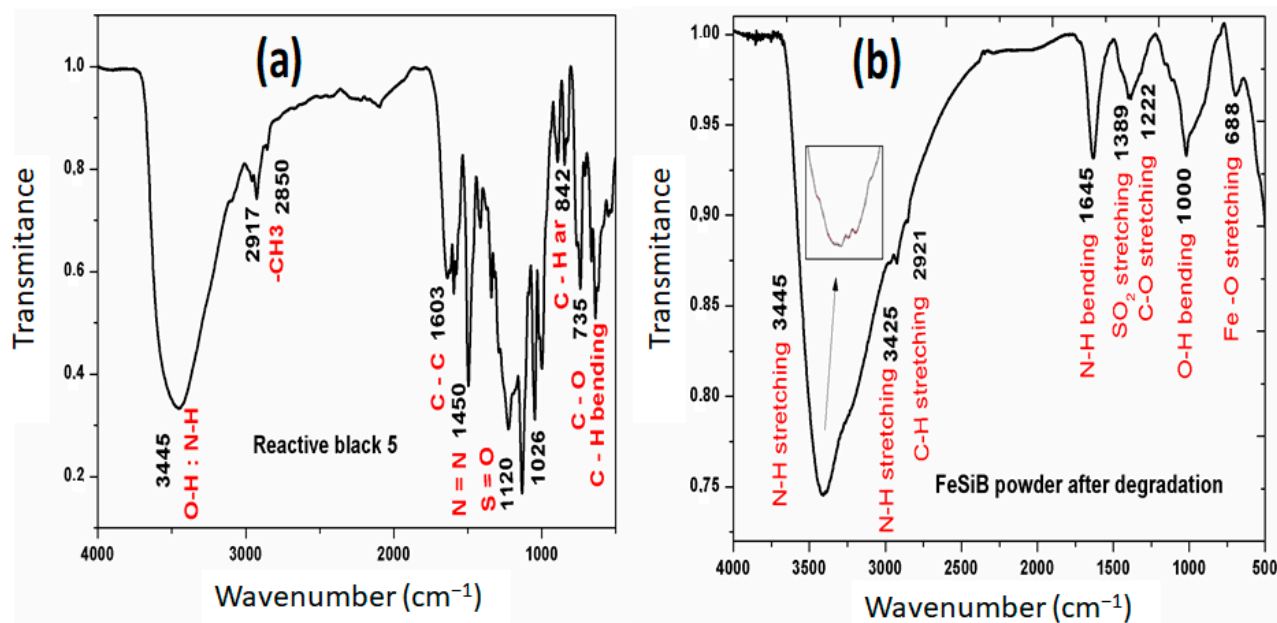
Figure 9. (**a**) FTIR spectra of the RB5 powder before the degradation reaction, and (**b**) FTIR spectra of the BM FeSiB powder after the degradation of Reactive Black 5.

Evidently, the FT-IR spectrum of the untreated sample dye shows characteristic peaks of –OH vibrational stretching at 3445 cm^{-1}, and –NH vibrational stretching, as in amines. The characteristic peaks at 2917 and 2850 cm^{-1} belong to the –CH$_3$ asymmetric and symmetric vibrational stretching and the –CH$_2$ asymmetric vibrational stretching. A characteristic peak for the C-C vibration of the aromatic ring appears at 1603 cm^{-1}. The most important peak appeared at 1450 cm^{-1}, representing the –N=N– azo linkages stretching. The sulfoxide nature of the RB5 was evident from the typical FT-IR peak that appeared at 1026 cm^{-1}. Comparatively, the FT-IR (Figure 9b), shows the functional groups of the reaction products, resulting from the reduction reaction, that have been adsorbed on the surface of the alloy powder. The observed spectral behavior is similar to that reported in other dye degradation studies [34,35]. The bands at 3445 cm^{-1} and 3425 cm^{-1} (N–H stretching), 1222 cm^{-1} (C–O stretching), and 1645 cm^{-1} (N–H bending) are present. The FT-IR after degradation indicates that some of the product contains a primary amine as a result of the reductive cleavage of the –N=N– bond. This is in agreement with the disappearance of the band at 1450 cm^{-1}, confirming the above-mentioned UV/V results concerning the cleavage of the azo bonds [11]. Above 2000 cm^{-1}, the extract exhibits the same antisymmetric and symmetric C–H stretching vibrations at about 2921 cm^{-1} as those of the –CH$_2$ groups in the short hydrocarbon chains of the by-products and the RB5 molecule. The absorption bands due to Fe–O symmetric stretching and O–H bending vibrations, occurring in the range of 620–680 cm^{-1} and 750–1000 cm^{-1}, respectively, were characteristic of the FeOOH phase as confirmed by XRD [36]. Figure 10 shows the UV-Vis after the degradation of RB5 by FeSiB powder; the absorption peak near 250 nm increased, implying the RB5 has already been converted into other substances after reduction by the FeSiB powders [37].

3.3. Secondary Treatment of Decolorized RB5 Aqueous Solution by Using Natural Adsorbents

The treatment of these substances was evaluated by different adsorbents, such as wood, graphene oxide, activated carbon, and pine powders. The experiment was performed with 0.04 g of adsorbents in 20 mL of the solution, continuously agitated for 1 h. Samples were removed and filtered, and the absorbance between 200 and 800 nm was measured by spectrophotometry. The absorption peak of the decomposition products at 248 nm does not shift for any of the UV–Vis spectra for wood, cork, and pine powders, indicating that the same decomposition products were formed by the FeSiB powder, regardless of the addition

of these adsorbents. On the other hand, the absorption peaks of the UV-Vis spectra of graphene oxide and activate carbon powders at 248 nm decrease, indicating the adsorption of the secondary products, especially when using OG. The absorption curve for the latter adsorbent shows that no aromatic derivatives are detected around 250 nm. It should be noted that the addition of GO and AC indicated the adsorption of the secondary products after the degradation processes of the RB5 solutions due to the availability of vacant active adsorption sites, resulting in improving the adsorption efficiency of the harmful substances (as shown in Figure 10).
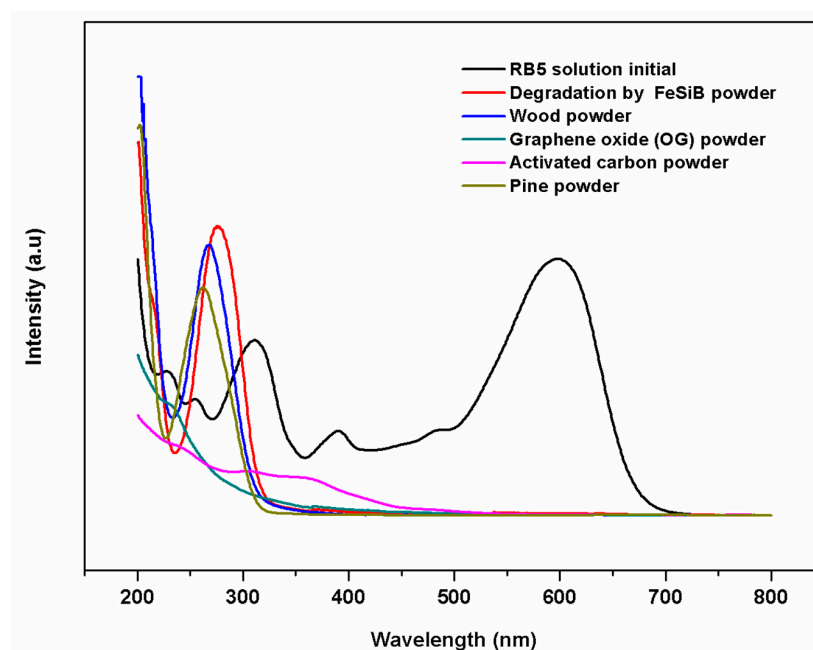
Figure 10. UV–Vis spectra of degradation RB5 solutions after adsorption by different adsorbents.

The absorption edges at 248 nm were used for the band gap energy calculation using the Kubelka–Munk function. The pine powder, wood powder, graphene oxide, and activated carbon powder show band gap energies of 5.3899, 5.2357, 3.7097, and 2.5047 eV, respectively. There is slight variation in the band of activated carbon compared to the other adsorbents, in which there is drastic reduction in the band gap from 5.2357 to 2.5047 eV (Figure 11), making the catalyst more efficient in the visible region. Hence the composite materials will enhance the photocatalytic degradation efficiency in visible light.

The degradation products formed during the degradation process were analyzed. Ben Mbarek et al. analyzed the HPLC-MS chromatogram of the RB5 dye in solution before the reduction by FeSiB. It consists of a broad peak eluting between 12.3–12.5 min. The major peaks of the RB5 dye correspond with a molecular weight of 822, 991 and 1061 [11].

Figure 12a,b displays the HPLC -MS analysis of the RB 5 dye dissolution at the final reduction treatment. Figure 10a shows peaks of different intensity between the times of 5.6 to 11 min. The time of the highest intensity peak is around 11 min, identified as 4-(2-hydroxyethyl)sulfonyl) phenol and m/z = 202. The other peaks of lower intensity correspond to a mixture of aromatic derivatives and other chemical compounds of smaller molecular weight from the fracture and degradation of the dye molecule. The chromatograms, after reduction by FeSiB (5 min), indicate the total reduction of the "–N=N–" azo bonding and the complete disintegration of the dye. The structures of the compounds obtained are identified from the fragmentation pattern data and the m/z values obtained following UPLC-MS analysis. The molecular identification is given in Table 3 as a function of the m/z values found. It can be deduced that the degradation of dyes proceeds via the cleavage of azo bonds giving rise to the formation of aromatic amines and other aromatic compounds as a result of molecular degradation. The degradation of azo dyes begins with

a reduction or cleavage of the azo bond, followed by a partial or total disintegration of the aromatic amines [38]. Similar analyses with HLPC-MS are carried out on the residual products from the adsorption process. The results of the +MS chromatogram are collected in Figure 10b. The structures of the compounds identified as a consequence of the adsorption process by GO, after reduction and fragmentation, of the dye dissolution are shown in Table 3. It can be concluded that the adsorption of aromatic products by GO is not complete because of the detection of 4-(2-hydroxyethyl)sulfonyl) phenol as a residual product. A quantitative analysis of residual phenol has not been carried out in this work. However, it is appropriate to point out that its UV-visible signal has not been detected.
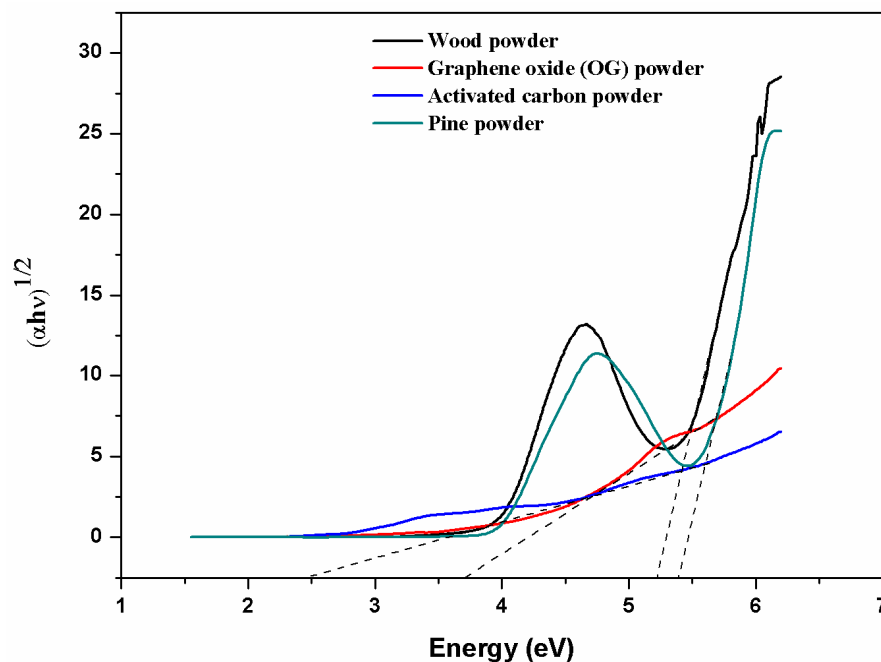

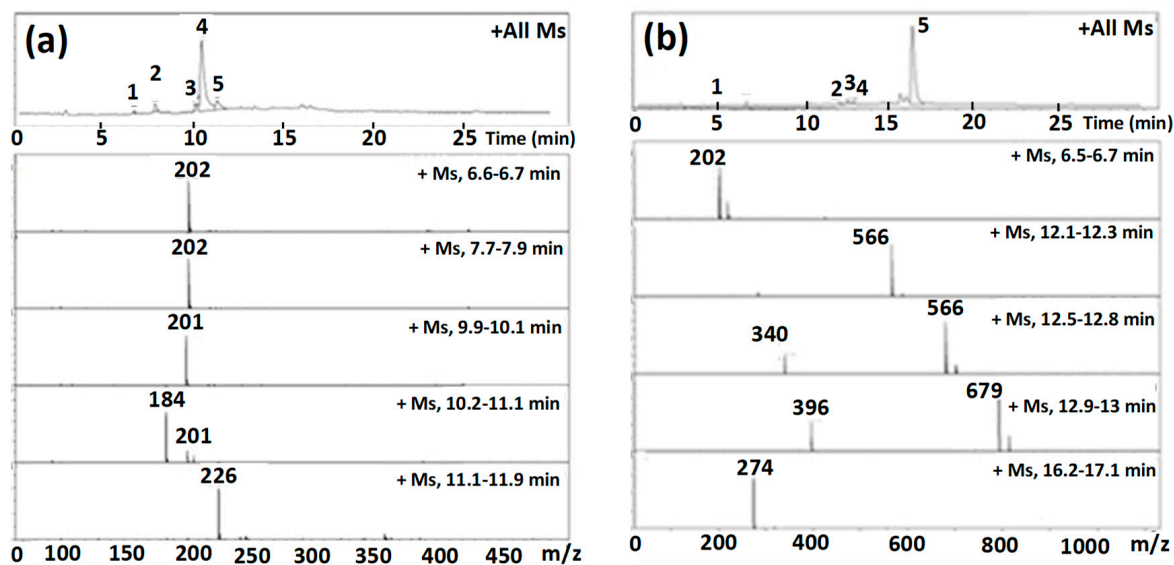**Figure 11.** Band gap energies of adsorbents after the reaction time.

Figure 12. (**a**) HPLC-MS chromatogram (+MS) of Reactive Black 5 solution after reduction by FeSiB powder. (**b**) HPLC-MS chromatogram (+MS) of Reactive Black 5 solution degraded by FeSiB powder after the adsorption process by OG powder.

Table 3. The degradation products of Reactive Black 5 after reduction by FeSiB and adsorption by OG powder in positive m/z values.

+MS	
Molecular Weight	**Molecular Compound**
HPLC-MS of Reactive Black 5 solution after degradation by FeSiB powder	
184	4-(vinylsulfonyl) phenol
201	4-(2-hydroxyethyl)sulfonyl) benzenoamina
202	4-(2-hydroxyethyl)sulfonyl) phenol
200	4-(2-aminoethyl)sulfonyl) benzenoamina
226	5-((4-hydroxyfenyl)sulfonyl)-2 penteno
HPLC-Ms of Reactive Black 5 solution degraded by FeSiB powder after the adsorption process by OG powder	
202	4-(2-hydroxyethyl)sulfonyl) phenol.

The results of this work indicate that the Fe80Si10B10 powder produced by mechanical alloying is an excellent and effective reductive agent for azo bonds. It only requires 3–5 min for complete discoloration. The crystal structure of the alloy is considered a key factor favoring the catalytic reduction of the azo functional group. The reducing agent is considered to be Fe^0, according to the results obtained by XRD. In the diffractogram of the powder after the reduction process, the formation of a new phase identified as Fe-OH is observed. The results confirm that the powder shows superior degradation capability and has higher degradation efficiency to degrade azo dyes than the commercial Fe powders (complete degradation of RB5 after 3 h [39]), attributed to the formation of numerous micro-batteries formed by different nanocrystalline environments, which favor the loss of electrons from the iron and promote the degradation process, as confirmed by Cheng et al. [40]. These favorable structures function in the same way as the amorphous ZVI and contribute to a high degradation efficiency. It is widely accepted that amorphous ZVI has a high degradation activity for azo dyes. However, a simple and cheap processing method (ball milling) can prepare crystalline powders with favorable structures and RB5 degradation efficiencies comparable to or higher than amorphous ZVI powders. Moreover, the secondary treatment was also studied as a result of the substances that appeared after the degradation of RB5 by FeSiB powder, detected by UV-Vis and HPLC-MS. The use of different adsorbents, such as wood, graphene oxide, activated carbon, and pine powders, was also studied. The results show that graphene oxide and activated carbon presented the best performances for the adsorption of the secondary products after the degradation of RB5.

4. Conclusions

$Fe_{80}Si_{10}B_{10}$ (at.%) powders were successfully fabricated by high-energy mechanical milling. The efficiency of $Fe_{80}Si_{10}B_{10}$ to degrade organic chemicals was investigated by evaluating the decolorization process of RB5 aqueous solutions. The ball-milled powder exhibited excellent degradation efficiency and high reaction rates, with a 100% dye removal of 40 mgL^{-1} dye solutions in less than three minutes. This high efficiency is associated to the nanocrystalline structure and the formation of multiple micro-batteries between the α-Fe solid solution and the Fe_3Si nanocrystalline phases, favoring the loss of electrons from iron and activating the chemical reduction. As an advantage, these metallic powders may be used as a low-cost, high-performance decolorizing method for textile wastewater pre-treatments. Based on the experimental results, a schematic reaction mechanism in aqueous basic medium has been proposed, which is based on the reducing power of iron. Thus, mechanical alloying is a useful technique in order to develop Fe-based powdered alloys for wastewater remediation.

The efficient removal of intermediate undesirable chemicals from reduction processes, primarily aromatic amines, is examined in the second step of the adsorption procedure. Adsorbents such as wood, graphene oxide, activated carbon, and pine particles were

employed. According to the data, graphene oxide and activate carbon performed the best for secondary product adsorption after RB5 degradation. The current study could be used as a model for environmental applications, such as industrial wastewater treatment, that use metallic powders produced by high-energy mechanical alloying. These findings may provide a highly efficient, low-cost, commercial method for azo dye wastewater treatment.

References

1. Mbarek, W.B.; Escoda, L.; Saurina, J.; Pineda, E.; Alminderej, F.M.; Khitouni, M.; Suñol, J.J. Nanomaterials as a Sustainable Choice for Treating Wastewater: A Review. *Materials* **2022**, *15*, 8576. [CrossRef] [PubMed]
2. Saravanan, R.; Gupta, V.K.; Mosquera, E.; Gracia, F.; Narayanan, V.; Stephen, A. Visible Light Induced Degradation of Methyl Orange Using β-Ag0.333V2O5 Nanorod Catalysts by Facile Thermal Decomposition Method. *J. Saudi Chem. Soc.* **2015**, *19*, 521–527. [CrossRef]
3. Mahmood, F.; Shahid, M.; Hussain, S.; Shahzad, T.; Tahir, M.; Ijaz, M.; Hussain, A.; Mahmood, K.; Imran, M.; Babar, S.A.K. Potential Plant Growth-Promoting Strain Bacillus Sp. SR-2-1/1 Decolorized Azo Dyes through NADH-Ubiquinone:Oxidoreductase Activity. *Bioresour. Technol.* **2017**, *235*, 176–184. [CrossRef]
4. Abramian, L.; El-Rassy, H. Adsorption Kinetics and Thermodynamics of Azo-Dye Orange II onto Highly Porous Titania Aerogel. *Chem. Eng. J.* **2009**, *150*, 403–410. [CrossRef]
5. Goudarzi, M.; Bazarganipour, M.; Salavati-Niasari, M. Synthesis, Characterization and Degradation of Organic Dye over Co_3O_4 Nanoparticles Prepared from New Binuclear Complex Precursors. *RSC Adv.* **2014**, *4*, 46517–46520. [CrossRef]
6. Roy, A.; Adhikari, B.; Majumder, S.B. Equilibrium, Kinetic, and Thermodynamic Studies of Azo Dye Adsorption from Aqueous Solution by Chemically Modified Lignocellulosic Jute Fiber. *Ind. Eng. Chem. Res.* **2013**, *52*, 6502–6512. [CrossRef]
7. Manivel, A.; Lee, G.J.; Chen, C.Y.; Chen, J.H.; Ma, S.H.; Horng, T.L.; Wu, J.J. Synthesis of MoO_3 Nanoparticles for Azo Dye Degradation by Catalytic Ozonation. *Mater. Res. Bull.* **2015**, *62*, 184–191. [CrossRef]
8. Nidheesh, P.V.; Gandhimathi, R.; Ramesh, S.T. Degradation of Dyes from Aqueous Solution by Fenton Processes: A Review. *Environ. Sci. Pollut. Res.* **2013**, *20*, 2099–2132. [CrossRef]
9. Singla, P.; Sharma, M.; Pandey, O.P.; Singh, K. Photocatalytic Degradation of Azo Dyes Using Zn-Doped and Undoped TiO_2 Nanoparticles. *Appl. Phys. A* **2013**, *116*, 371–378. [CrossRef]
10. AboliGhasemabadi, M.; Ben Mbarek, W.; Casabella, O.; Roca-Bisbe, H.; Pineda, E.; Escoda, L.; Suñol, J.J. Application of Mechanically Alloyed MnAl Particles to De-Colorization of Azo Dyes. *J. Alloys Compd.* **2018**, *741*, 240–245. [CrossRef]
11. Ben Mbarek, W.; Pineda, E.; Escoda, L.; Suñol, J.J.; Khitouni, M. High Efficiency Decolorization of Azo Dye Reactive Black 5 by Ca-Al Particles. *J. Environ. Chem. Eng.* **2017**, *5*, 6107–6113. [CrossRef]
12. Ben Mbarek, W.; Saurina, J.; Escoda, L.; Pineda, E.; Khitouni, M.; Suñol, J.-J. Effects of the Addition of Fe, Co on the Azo Dye Degradation Ability of Mn-Al Mechanically Alloyed Powders. *Metals* **2020**, *10*, 1578. [CrossRef]
13. McMullan, G.; Meehan, C.; Conneely, A.; Kirby, N.; Robinson, T.; Nigam, P.; Banat, I.; Marchant, R.; Smyth, W. Microbial Decolourisation and Degradation of Textile Dyes. *Appl. Microbiol. Biotechnol.* **2001**, *56*, 81–87. [CrossRef] [PubMed]
14. Peternel, I.T.; Koprivanac, N.; Božić, A.M.L.; Kušić, H.M. Comparative Study of UV/TiO_2, UV/ZnO and Photo-Fenton Processes for the Organic Reactive Dye Degradation in Aqueous Solution. *J. Hazard. Mater.* **2007**, *148*, 477–484. [CrossRef] [PubMed]
15. Shih, Y.-H.; Tso, C.-P.; Tung, L.-Y. Rapid Degradation of Methyl Orange with Nanoscale Zerovalent Iron Particles. *J. Environ. Eng. Manag.* **2010**, *20*, 137–143.
16. Bokare, A.D.; Chikate, R.C.; Rode, C.V.; Paknikar, K.M. Iron-Nickel Bimetallic Nanoparticles for Reductive Degradation of Azo Dye Orange G in Aqueous Solution. *Appl. Catal. B Environ.* **2008**, *79*, 270–278. [CrossRef]
17. Jia, Z.; Duan, X.; Zhang, W.; Wang, W.; Sun, H.; Wang, S.; Zhang, L.C. Ultra-Sustainable $Fe_{78}Si_9B_{13}$ Metallic Glass as a Catalyst for Activation of Persulfate on Methylene Blue Degradation under UV-Vis Light. *Sci. Rep.* **2016**, *6*, 38520. [CrossRef]

18. Lutterotti, L. MAUD CPD Newsletter (IUCr), No. 24, 2000.-References-Scientific Research Publishing. Available online: https://www.scirp.org/%28S%28czeh2tfqyw2orz553k1w0r45%29%29/reference/referencespapers.aspx?referenceid=782192 (accessed on 26 April 2022).

19. Gnanamoorthy, G.; Ali, D.; Yadav, V.K.; Dhinagaran, G.; Venkatachalam, K.; Narayanan, V. New Construction of Fe$_3$O$_4$/RGO/ZnSnO$_3$ Nanocomposites Enhanced Photoelectro Chemical Properties. *Opt. Mater.* **2020**, *109*, 110353. [CrossRef]

20. Gnanamoorthy, G.; Muthamizh, S.; Sureshbabu, K.; Munusamy, S.; Padmanaban, A.; Kaaviya, A.; Nagarajan, R.; Stephen, A.; Narayanan, V. Photocatalytic Properties of Amine Functionalized Bi2Sn2O7/RGO Nanocomposites. *J. Phys. Chem. Solids* **2018**, *118*, 21–31. [CrossRef]

21. Ben Mbarek, W.; Azabou, M.; Pineda, E.; Fiol, N.; Escoda, L.; Suñol, J.J.; Khitouni, M. Rapid Degradation of Azo-Dye Using Mn-Al Powders Produced by Ball-Milling. *RSC Adv.* **2017**, *7*, 12620–12628. [CrossRef]

22. Sarsamb, L.A.; Mohammeda, D.H. Spectrophotometric Determination of Benzocaine by Azo-Dye Formation Reaction. *J. Univ. Anbar Pure Sci.* **2011**, *5*, 24–30. [CrossRef]

23. Al-Safar, R.S.; Othman, N.S. Spectrophotometric Determination of Sulphacetamide Sodium via Diazotization and Coupling Reaction. *IOP Conf. Ser. Mater. Sci. Eng.* **2020**, *928*, 052017. [CrossRef]

24. Bonicamp, J.M.; Martin, K.L.; McBride, G.R.; Clark, R.W. Beer's Law Is Not a Straight Line: Amplification of Errors by Transformation. *Chem. Educ.* **1999**, *4*, 81–88. [CrossRef]

25. Valcarcel, M.I. *Principles of Analytical Chemistry*; Springer: Berlin/Heidelberg, Germany, 2000.

26. Fan, J.; Guo, Y.; Wang, J.; Fan, M. Rapid Decolorization of Azo Dye Methyl Orange in Aqueous Solution by Nanoscale Zerovalent Iron Particles. *J. Hazard. Mater.* **2009**, *166*, 904–910. [CrossRef]

27. Xie, S.; Huang, P.; Kruzic, J.J.; Zeng, X.; Qian, H. A Highly Efficient Degradation Mechanism of Methyl Orange Using Fe-Based Metallic Glass Powders. *Sci. Rep.* **2016**, *6*, 21947. [CrossRef]

28. Chen, J.; Zhu, L. Heterogeneous UV-Fenton Catalytic Degradation of Dyestuff in Water with Hydroxyl-Fe Pillared Bentonite. *Catal. Today* **2007**, *126*, 463–470. [CrossRef]

29. Xie, S.H.; Peng, G.Q.; Tu, X.M.; Qian, H.X.; Zeng, X.R. Fe-Based Powders Prepared by Ball-Milling with Considerable Degradation Efficiency to Methyl Orange Compared with Fe-Based Metallic Glasses. *Acta Metall. Sin. (Engl. Lett.)* **2018**, *31*, 1207–1214. [CrossRef]

30. Wang, P.; Wang, J.Q.; Li, H.; Yang, H.; Huo, J.; Wang, J.; Chang, C.; Wang, X.; Li, R.W.; Wang, G. Fast Decolorization of Azo Dyes in Both Alkaline and Acidic Solutions by Al-Based Metallic Glasses. *J. Alloys Compd.* **2017**, *701*, 759–767. [CrossRef]

31. Samiee, S.; Goharshadi, E.K.; Nancarrow, P. Successful Degradation of Reactive Black 5 by Engineered Fe/Pd Nanoparticles: Mechanism and Kinetics Aspects. *J. Taiwan Inst. Chem. Eng.* **2016**, *67*, 406–417. [CrossRef]

32. Feng, W.; Nansheng, D.; Helin, H. Degradation Mechanism of Azo Dye C. I. Reactive Red 2 by Iron Powder Reduction and Photooxidation in Aqueous Solutions. *Chemosphere* **2000**, *41*, 1233–1238. [CrossRef] [PubMed]

33. Tang, C.-B.; Wen, F.-R.; Chen, H.-X.; Liu, J.-J.; Tao, G.-Y.; Xu, N.-J.; Xue, J.-Q. Corrosion Characteristics of Fe$_3$Si Intermetallic Coatings Prepared by Molten Salt Infiltration in Sulfuric Acid Solution. *J. Alloys Compd.* **2019**, *778*, 972–981. [CrossRef]

34. Neoh, C.H.; Lam, C.Y.; Lim, C.K.; Yahya, A.; Bay, H.H.; Ibrahim, Z.; Noor, Z.Z. Biodecolorization of Recalcitrant Dye as the Sole Sourceof Nutrition Using Curvularia Clavata NZ2 and Decolorization Ability of Its Crude Enzymes. *Environ. Sci. Pollut. Res.* **2015**, *22*, 11669–11678. [CrossRef] [PubMed]

35. Bilal, M.; Rasheed, T.; Iqbal, H.M.N.; Hu, H.; Wang, W.; Zhang, X. Toxicological Assessment and UV/TiO2-Based Induced Degradation Profile of Reactive Black 5 Dye. *Environ. Manag.* **2018**, *61*, 171–180. [CrossRef] [PubMed]

36. Vernekar, D.; Jagadeesan, D. Tunable Acid–Base Bifunctional Catalytic Activity of FeOOH in an Orthogonal Tandem Reaction. *Catal. Sci. Technol.* **2015**, *5*, 4029–4038. [CrossRef]

37. Liu, X.; Liang, M.; Liu, M.; Su, R.; Wang, M.; Qi, W.; He, Z. Highly Efficient Catalysis of Azo Dyes Using Recyclable Silver Nanoparticles Immobilized on Tannic Acid-Grafted Eggshell Membrane. *Nanoscale Res. Lett.* **2016**, *11*, 440. [CrossRef]

38. Mané, U.; Gurav, P.; Deshmukh, A.; Govindwar, S. Degradation of Textile Dye Reactive Navy-Blue Rx (Reactive Blue–9) by an Isolated Actinomycete Streptomyces Krainskii SUK-5. *Malays. J. Microbiol.* **2008**, *4*, 1–5. [CrossRef]

39. Chatterjeea, S.; Limb, S.R.; Woo, S.H. Removal of Reactive Black 5 by zero-valent iron modified with various surfactants. *Chem. Eng. J.* **2010**, *160*, 27–32. [CrossRef]

40. Chen, S.Q.; Li, M.; Ma, X.Y.; Zhou, M.J.; Wang, D.; Yan, M.Y.; Li, Z.; Yao, K.F. Influence of Inorganic Ions on Degradation Capability of Fe-Based Metallic Glass towards Dyeing Wastewater Remediation. *Chemosphere* **2021**, *264*, 128392. [CrossRef]